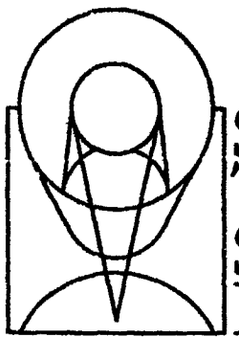

SPACE TELESCOPE SCIENCE INSTITUTE

PREPRINT SERIES
No. 293

ACCRETION SHOCK GEOMETRIES IN THE MAGNETIC VARIABLES

H. S. Stockman

July 1988

SPACE TELESCOPE SCIENCE INSTITUTE
3700 San Martin Drive Baltimore, MD 21218

Operated by the Association of Universities for Research in Astronomy, Inc., for the National Aeronautics and Space Administration

Accretion Shock Geometries in the Magnetic Variables

by

H. S. Stockman

Space Telescope Science Institute[1]

3700 San Martin Drive

Baltimore, Maryland 21218

Presented at the 1987 Vatican Workshop on Circumstellar Polarization.

To be published in "Polarized Radiation of Circumstellar Origin", 1988 in press

1. Operated by the Association of Universities for Research in Astronomy, Inc., for NASA.

ABSTRACT

The first self-consistent shock models for the AM Herculis-type systems were successful in identifying the dominant physical processes and their signatures. These homogenous shock models predict unpolarized, Rayleigh-Jeans optical spectra with sharp cutoffs and rising polarizations as the shocks become optically thin in the ultraviolet. However, the observed energy distributions are generally flat with intermediate polarizations over a broad optical band. These and other observational evidence support a non-homogenous accretion profile which may extend over a considerable fraction of the stellar surface. We review both the fundamental assumptions underlying the canonical 1-D shock model and the extension of this model to inhomogenous accretion shocks, for both radial and linear structures. We also examine the observational evidence for "tall" shocks and find little evidence for relative shock heights in excess of, $h/R_1 \gtrsim 0.1$. For several systems, upper limits to the shock height can be obtained from either X-ray or optical data. These lie in the region $h/R_1 \lesssim 0.01$ and are in general agreement with the current physical picture for these systems. The quasi-periodic optical variations observed in several magnetic variables may eventually prove to be a major aid in further understanding their accretion shock geometries.

1.0 INTRODUCTION

The discovery of circular polarization in AM Herculis twelve years ago (Tapia 1977) introduced a new observational field of time-resolved circular polarimetry of the Cataclysmic Variables and new opportunities for studying the physics of accretion binary systems. While tentative observations of circular polarization in DQ Her by Kemp *et al* (1974) had suggested the presence of a magnetic white dwarf primary, the strong circular polarizations found in the AM Her systems ($V \sim 8-40\%$) could only originate from harmonic cyclotron emission in strong magnetic fields, $B > 10-20 \times 10^6$ gauss (MG, see Lamb 1985, and previous papers in this volume.) Two remarkable properties of these systems make them particularly valuable for studying high energy astrophysics: the white dwarf rotation is perfectly synchronized with the companion star's orbital motion and the magnetic field controls the accretion flow, funneling it into a small area of the white dwarf's surface (see Lamb, 1988). As a result, the synchronous variations of the optical flux, its polarization properties, and the hard and soft X-ray flux promised to elucidate the physics of the interface between the infalling material and the stellar surface: the accretion shock. Indeed, the initial shock models by Lamb and Masters (1979) successfully explained the qualitative features of the early observations. However, the improved X-ray and optical coverage and more quantitative analysis progressively indicated that the actual accretion geometries and shock conditions were more complicated (Wickramasinghe, 1988).

In this paper, we discuss several modifications to the canonical shock model which are both reasonable and appear necessary to explain the observational data summarized by Bailey, Piirola, Schmidt, Beuermann and others in this volume. Since a rigorous exposition of the shock physics is unjustified by the simplifying assumptions required to complete our mental picture of these shocks, we emphasis both the feasibility of the various effects and the evidence which supports their presence.

2.0 CANONICAL SHOCK MODEL

Lamb and Masters (1979) created a series of energetically self-consistent models of accretion shocks for field strengths between 0.1 MG $\leq B \leq$ 100 MG and a range of white dwarf masses, $0.4M_{\odot} \leq M_1 \leq 1.4M_{\odot}$. These models assumed a cylindrically symmetric, homogenous accretion flow and a "thin" shock, ie. the height of the shock, h, was small compared to the half-width of the shock, r_s, which in turn was small compared to the radius of the white dwarf, R_1, or $h \ll r_s \ll R_1$ (see Figure 1a). While the model results often fell outside these regimes, this approximation permitted the solution and extension of the local shock characteristics without recourse to a specific, multidimensional model. As we indicate in Sections 3-4 and is foreshadowed in Figures 1b&1c, the physical consequences of relaxing these and other assumptions are significant and may resolve current discrepancies between the canonical model predictions and observations.

The canonical model shock characteristics are parameterized by the white dwarf mass, M_1, and implied radius, R_1, a constant magnetic field strength, B, and the local accretion density, $\dot{m}$, which is often stated in relation to the normalized accretion luminosity, L/f, where f is the fractional coverage of the stellar surface by the accretion shock:

$$\frac{L}{f} = \frac{4GM_1\dot{M}R_1}{r_s^2} \tag{1}$$

and

$$\dot{M} = \dot{m}\pi r_s^2. \tag{2}$$

The pre-shock density of the infalling gas, ρ_1, can be obtained from $\dot{m} = \rho_1 v_1$, where v_1 is approximately the free-fall velocity, $v_1 = (2GM_1/R_1) \sim 7.3 \times 10^3 km/s(M/R)^{1/2}$. ($M = M_1/M_{\odot}$ and $R = R_1/5 \times 10^8$ cm are convenient scaling factors.) In the canonical model, the density behind the shock, ρ_2, is given by the jump conditions for a strong shock while the velocity behind the shock, v_2 is obtained from the continuity equation.

$$\rho_2 = 4\rho_1 \tag{3}$$

and

$$\rho_2 v_2 = \rho_1 v_1 \tag{4}$$

yielding,

$$v_2 = \frac{1}{4}v_1. \tag{5}$$

In the spirit of the homogeneous shock approximation and, therefore, neglecting temperature structure and thermal conduction, the shock height can be determined by the requirement that a parcel of shocked gas must cool by the time it reaches the base of the shock or

$$t_{cool} \sim \frac{GM_1/R_1}{\phi(\rho_2, T_e, h)} \tag{6}$$

and

$$t_{cool} = \frac{h}{v_2}. \tag{7}$$

Here $\phi(\rho, T_e, h)$ is the specific cooling rate at an electron temperature T_e.

2.1 Bremsstrahlung-Dominated Shocks

For magnetic white dwarfs, with $M_1 \leq 1.0 M_\odot$, the dominant cooling mechanisms are bremsstrahlung emission and optically thick cyclotron emission. For a fixed field strength, the two cooling regimes and resultant structures depend on the accretion rate. For high $\dot{m}$, or $L/f > L/f_{crit}$, bremsstrahlung is the dominant coolant (Regime I in Lamb and Masters 1979). Typically in these shocks, $t_{cool} \gg t_{ie}$, the exchange time between the electrons and the shocked nuclei, and $T_i = T_e = T_s = 64keV(M/R)$ (Imamura *et al* 1987). Since $\phi_{brems} \propto \rho_2 T_e^{1/2}$, for a given M/R,

$$t_{cool} \propto h \propto \rho_2^{-1} \propto (L/f)^{-1}. \tag{8}$$

The cyclotron opacity is a strong function of the magnetic field strength, the temperature, and the frequency. Ignoring angular beaming effects, the emerging flux from an isothermal thin shock will appear as a Rayleigh-Jeans spectrum up to a critical frequency, ν_{crit}, above which the spectrum is truncated. While a quantitative calculation of the cyclotron emission requires an integration over angles, polarizations, and the inevitable temperature structure in the shock, we will use the simplest approximations of Dulk and Marsh(1982) for an emergent angle of 45° to illustrate the general behavior of the cyclotron cooling. Using the nomenclature already introduced, they obtain the critical frequency of the emergent radiation of:

$$\nu_{crit} \sim 2.1 \times 10^{15} B_{30}^{0.9} kT_{50}^{0.7} \tau_e^{0.1} \text{ Hz}. \tag{9}$$

Here, $B_{30} = B/30$ MG, $kT_{50} = kT_e/50$ keV, and τ_e is the optical depth of the shock to Compton scattering. Note the strong dependence on temperature and field strength and the extremely weak dependence on surface density. For the bremsstrahlung-dominated shocks, $\tau_e \sim 0.3\rho_2 h \sim 0.3(M/R)^{1/2}$. Thus, with our assumptions, the emergent cyclotron flux and spectrum for a bremsstrahlung-dominated shock has a characteristic brightness temperature, T_s, and cutoff frequency, ν_{crit}, given above with *no dependence* on accretion density.

Integrating the Rayleigh-Jeans spectrum to the critical frequency, we obtain the local cyclotron luminosity as:

$$l_{cyc} = \frac{2\pi}{3c^2} kT \nu_{crit}^3, \tag{10}$$

and the total cyclotron luminosity for a bremsstrahlung-dominated shock as:

$$L/f_{crit}(B, M/R) \sim 0.1 L_{Edd} (M/R)^{2.25} R_1 B_{30}^{2.7}. \tag{11}$$

2.2 Cyclotron-Dominated Shocks

For field strengths much greater than typical AM Her field strengths, $B \gg 30$ MG, or for accretion flows substantially below the local Eddington limit, $L_{Edd} \sim 1.4 \times 10^{38} M$ erg/s, the dominant cooling mechanism is optical cyclotron emission. ($\phi \propto T_e \nu_{crit}^3 / \tau_e$). Generally, in the cyclotron-dominated regime, $t_{cool}(T_s) \lesssim t_{ie}$ and the electron and ion temperatures are driven out of equilibrium. This corresponds to Regime II in Lamb and Masters (1979). To obtain the electron temperature, we extend the cooling time argument to cover the electron-ion cooling.

$$t_{cool}(T_e) = t_{ie}(T_e) = \frac{h}{v_2}. \tag{12}$$

Here t_{ie} is obtained from the Coulomb exchange time. For $T_e/T_i \gg m_e/m_i$ and $T_e \ll T_i$, (*cf* Imamura *et al* 1987 but also Section 2.3),

$$t_{ie}(T_e) \propto \frac{T_e^{3/2}}{\rho_2}. \tag{13}$$

Thus, in this regime, the electron temperature is regulated by the cyclotron cooling and ion-electron exchange. The post-shock velocity and density are still given by the strong shock condition but the height and temperature are given by the following approximate scaling relations:

$$T_e \sim T_s \left[\frac{(L/f)}{(L/f)_{crit}} \right]^{0.3} \tag{14}$$

$$h/R \sim 0.003 \left[\frac{L/f}{L_{Edd}} \right]^{-0.56} (M/R)^2 B_{30}^{-1.2} M^{0.56}. \tag{15}$$

Despite the coupled nature of these shock equations, the strong temperature dependence of the cyclotron opacity essentially adjusts the temperature to obtain the ν_{crit} required to radiate the accretion luminosity, while the resulting ion-electron coupling time sets the height.

2.3 Extensions of the Canonical Model

As pointed out by Lamb and Masters(1979) and Masters (1978), the two-temperature model breaks down at very low accretion densities when $t_{cool} \lesssim t_{ii}$, the ion-ion coupling time. In this regime (Regime III), the electron-ion coupling becomes stronger than the ion-ion coupling and the shock is no longer self-supporting. Stockman and Lubenow (1987) have extended the canonical model into this regime by picturing the infalling ions as an interpenetrating fluid into a cooling layer. In this scenario, the relationship between ρ_1 and ρ_2 is given by a pressure relation:

$$\rho_1 (v_1)^2 \sim n_{i2} k T_{i2} + n_{e2} k T_{e2} \tag{16}$$

and

$$t_{ii} \sim t_{cool} = h/v_2 \tag{17}$$

Here t_{ii} is the momentum exchange time between the incoming ions and the ions in the cooling layer. To obtain a self-consistent calculation, a full network of energy exchange between the infalling ions and the species in the cooling layer is required. In practise, however, the electron temperature continues to be a primary function of the accretion luminosity and closely follows the temperature relation for Regime II. The shock height is a more complicated function of the accretion rate as can be seen in Figure 2. In this figure, the model results for $M_1 = 0.4$ and $1.0 M_\odot$ and $B = 10$ and 30 MG are displayed. The non-monotonic behavior in the shock height is due to the initial onset of Regime II, where the ion-electron coupling time is inversely proportional to $\Delta T_{ie} = T_i - T_e$, which increases rapidly with lower L/f. Indeed, the shock never reaches the assymptotic formula given above for Regime II before the onset of the non- hydrodynamic shock regime (Regime III). This result differs somewhat from that of Lamb and Masters (1979), who assumed $T_i \sim 2T_e$ for Regime II. While the integrated energy distribution is not sensitive to the shock height, self- eclipses by the white dwarf limb will produce qualitatively different light curves for the two models.

Also shown in Figure 2 are lines indicating the criteria, $L = L/f \times (h/R_1)^2$. For radial, "pillbox" type shocks (Fig.1a), shock heights exceeding these contours for a given luminosity violate the thin-shock assumption (see Section 3.1). We note that the combination of strong radiation transfer effects, coupled with the rapid change in the shock height near the onset of Regime II may be a strong mechanism for a global shock instability (see Section 4.3).

3.0 NON-HOMOGENEOUS SHOCK MODELS

While the dominant coolants and plasma effects vary in a complicated fashion according to the local accretion rate as described in Section 2, the fundamental characteristics of the emergent radiation are easily stated. For all regimes excepting the directly heated photosphere, the critical cyclotron frequency decreases as the local accretion rate declines. For homogeneous shock models (as illustrated in Figure 1a), the observed cyclotron flux should drop precipitously at frequencies above the critical frequency and show strong polarizations characteristic of an optically thin plasma. The energy distribution at lower frequencies (longer wavelengths) should be approximately Rayleigh-Jeans and show relatively little polarization. The difficulty of reconciling these predictions with the flatter observed energy distribution, $f(\nu) \propto \nu^{-1}$ and moderate broadband polarization of AM Her was recognized soon after Lamb and Masters 1979 publication and the confirmation of the fundamental role of cyclotron harmonics as evidenced by the low field strength in VV Pup (Visvanathan and Wichramasinghe 1979) and AM Her (Schmidt, Stockman and Margon 1981).

In general, the conflict between the simple homogeneous model predictions and the observed characteristics was addressed by assuming a site for the optical radiation separate from the origins of the X-ray flux: either above the bremsstrahlung-dominated shock or in a much larger and cooler region. Liebert and Stockman (1985) first suggested a non-homogeneous shock geometry and noted that power-law energy distributions could be obtained if the local accretion rate were to decline as a power- law away from the "core" of the shock. This picture was developed further by Schmidt, Stockman, and Grandi (1983), who also considered exponential and Gaussian declines in the local accretion rate. In numerical simulations covering a broad class of exponential and power-law dependencies, Stockman and Lubenow (1987) have confirmed the simple analytical results of Schmidt, Stockman, and Grandi (1983). In

this section, we summarize the elements of the non-homogeneous shock models and some of their far-reaching consequences.

3.1 Variable Accretion Densities

In the simplest extension of the homogeneous shock model, we consider the local accretion rate $\dot{m}(r)$ to be a monotonically declining function of the radial distance,r, from the "core" of the shock. We can extend the "thin-shock" assumption so that $h(r) \ll l \ll R_1$, where l is a characteristic scale for change, $l \sim (dln(\dot{m}(r))/dr)^{-1}$. With this assumption, the structure of the shock at a given radius r is simply that of the homogeneous model and the observed characteristics of the shock can be obtained by integrating over the characteristics from the core of the shock to its outermost boundary, r_{max}. In particular, the total luminosity of the shock is given by

$$L = \int_o^{r_{max}} \frac{GM_1\dot{m}(r)}{R_1} 2\pi r dr. \tag{17}$$

The observed cyclotron flux at a frequency, ν, is proportional to

$$f(\nu) \propto \nu^3 \int_0^{r(\nu)} T(r) 2\pi r dr. \tag{18}$$

where $r(\nu)$ is the radius at which the shock becomes optically thin to cyclotron radiation at the frequency, ν. Similar relations can be obtained for the integrated hard and soft X-ray spectra using the formulae presented in Section 2. Before discussing the qualitative results for various accretion rate "profiles," it is valuable to consider the limitations imposed by the thin-shock assumption.

As shown in Section 2, the shock height can be comparable to the shock width or characteristic scale length, l, for accretion luminosities characteristic of the AM Her variables. In the bremsstrahlung regime, the principle effect will be a slightly larger and somewhat cooler soft X-ray region underlying the shock. In the cyclotron dominated regime, however, cyclotron cooling will be enhanced by radiation channeling through the sides of the column; both radially inward *above* the higher density core and outward *through* the cooler shock region. The primary effect of the enhanced cooling will be to suppress the electron temperature and, subsequently, to reduce the shock height.

In accretion geometries with large shock regions, $l \sim R_1$, both the variation in the surface magnetic field strength and the surface and field curvature should be considered. The latter effects are described in Section 4.2 and have been modeled by Wickramasinghe and Ferrario (1988).

3.2 Power-law Accretion Profiles

While the observed flux from exponential or gaussian accretion profiles are essentially identical to those for the appropriate "pillbox" geometry, power-law accretion profiles can produce dramatically different energy distributions. These can be illustrated by the following example from Stockman and Lubenow (1987) which approximates the active state of AM Her: $L = 10^{33} erg/s, (L/f) = 10^{38} erg/s, M = 0.8$, and $B = 20$ MG. The adopted accretion profile is $\dot{m}(r) \propto 1/(1+r^2)$. Figure 3 shows the integrated energy distribution for this model compared to that for a gaussian accretion profile, while Figure 4 shows the variation in shock characteristics versus radius for the power-law model.

Several features illustrate the nature of the accretion profile models. First, the bremsstrahlung-dominated "core" of the shock provides most of the hard and soft X-ray flux. Since the electron temperature and surface density are relatively constant, the optical cyclotron from this region is characterized by a constant critical frequency and area-limited flux. Second, in the "wings" or "halo" of the shock, the peak wavelength and shock height increase for larger radii and smaller $\dot{m}(r)$. A qualitative treatment of the radiation channeling has been included in these models and yields a smoother variation with shock height than that displayed in Figure 2. For differing power-law profiles, the resulting energy distributions exhibit different power law characteristics–both in the optical cyclotron portion of the spectrum and in the reprocessed ultraviolet portion of the spectrum. The predictions of the quadratic form are particularly interesting since they provide both a red, $f(\nu) \propto \nu^{-1}$ spectrum in the visible and an "ultraviolet excess" in the IUE band-pass. This agrees qualitatively with the bright-phase observations of AM Her. Steeper power-law profiles result in steeper, gaussian-like spectra, while flatter power-laws produce flat optical spectra. Recently, Wickramasinghe and Ferrario (1988, and this volume) have studied the cyclotron intensity and polarization from various shock profiles, using 3-D radiation transfer calculations. They also obtain "flat" optical spectra, confirming our pseudo-2D calculations, and find good agreement with the observed broadband polarizations. (The quadratic accretion profile best compares to their model with $\delta \sim 4$ with the linearly declining temperature.)

3.4 Extension to Linear Structures

Recent analyses of x-ray data (Beuermann *et al.* 1987), and optical data by Schmidt (1988) suggest that the accretion shocks may be more linear or arc-like than circular. This structure is shown schematically in Figure 1c. The non-homogeneous model can be extended to these structures by choosing a functional form for $\dot{m}(x)$ which depends on the perpendicular distance , x, from the center of the arc. Using the same thin-shock assumptions, we would obtain virtually identical energy distributions for the AM Her model using the linear form of the power-law profile, $\dot{m}(x) \propto 1/(1+x)$. Like the quadratic form, the linear form must be truncated for $x \sim R_1$, either by the onset of direct-photospheric heating by the dilute accretion stream, or, perhaps, by physical limits to the out-of-plane dispersion in the unthreaded accretion stream.

3.5 Implications of Power-Law Accretion Profiles

The qualitative agreement between the results of the inhomogeneous shock model and X-ray and optical observations, in addition to many independent analyses which support an X-ray core and optical halo structure for the accretion shock (e.g., Beuermann 1988), provide strong support for diffuse accretion over much of the surface of the white dwarf. In Figure 1b, we indicate schematically how such an accretion shock might appear. The "inevitable" downturn in the visible shock would be due to the onset of direct-heating of the white dwarf photosphere. While the cyclotron emission may be confined to a fraction of the stellar surface, accretion and photospheric reradiation in the mid-ultraviolet may occur over much of the entire star. To explain the UV "bump" in AM Her, the derived coverage for the halo radiation, $f \gtrsim 0.1$, implies that significant portions of the accretion stream remain unthreaded until very near the white dwarf surface, $R_{thread} \sim 3 - 5R_1$. Since the ballistic trajectory of the accretion stream has a typical minimum radius of approach of $R_b \sim 10R_1$ (Lubow and Shu 1975), significant out-of plane dispersion must occur before the accretion stream is completely threaded.

4.0 OBSERVATIONAL CONSTRAINTS ON SHOCK STRUCTURES

The discussions in Sections 2-3 suggest that the shock structures for the AM Herculis magnetic variables may be more complicated than those described in the initial models. Not only are several regimes of shock-physics potentially important, but many or all of these regimes may contribute to the observed optical, ultraviolet, soft X-ray and hard X-ray fluxes. To explain the relative strengths and time behavior of these wavebands, one may resort to complicated structures with little understanding of their underlying up- stream origins. It is important, therefore, to observationally test some of the underlying assumptions and results of these models before continuing additional parameterized studies or using model fits to draw strong conclusions regarding the accretion stream or threading region. In this section, we review the current observational evidence relative to a fundamental result of the shock models outlined in Section 2: the shock height, h. In a number of sources, the hard X-ray and optical variations (polarimetric and photometric) generally support the qualitative picture developed here. In other objects, the quasi-stable oscillations offer great potential as a probe of the shock structure.

4.1 Compact Bremsstrahlung Accretion Cores

Several lines of evidence (Beuermann, 1988*a*), as well as the results of model fits to the observed energy distributions of AM Her and E2003+225 (Stockman and Lubenow 1987) indicate that the central high density accretion luminosities approach the local Eddington luminosity, $L/f \sim L_{Edd} \sim 1 - 2 \times 10^{38}$ erg/s. In this regime, Compton cooling becomes a dominant cooling mechanism, lowering the shock temperature and height (Imamura *et al* 1987). Radiation pressure will not play a major role if the core of the shock is small compared to the stellar radius, $hL/(R_1 L_{Edd}) \ll 1$. However, as suggested by Beuermann (1988*b*), the ram pressure of the accretion stream can compress the photosphere of the white dwarf by many scale heights. Coupled with the low X-ray shock heights and the power-law accretion profiles, this can create "dimples" or "trenches" in the white dwarf atmosphere which can absorb and collimate the X-ray and the beamed, ultraviolet cyclotron emission from the core. Figure 5 shows a cross section for such a trench. The criteria for significant collimation is that the central X-ray shock height is less than the ram depth or

$$h_x(\dot{m}(r)) < d(\dot{m}(r)), \tag{19}$$

and that the change in the ram depth across the core of the shock is greater than the half-width of the core, r_s. Using the more accurate results of Imamura *et al* (1987) for this regime ($L/f \sim 0.1 - 1\ L_{EDD}$, $M \sim 1$), we can approximate the X-ray shock half-height (appropriate for 3–10 keV band) as:

$$h_x/R_1 \sim 1.5 \times 10^{-4} L_{Edd}/L. \tag{20}$$

The ram depth is approximated by equating the accretion ram pressure to the underlying photospheric pressure, or

$$\dot{m} v_1 \sim 2 n_2 k T_s \sim 2 n_{phot} k T_{phot}. \tag{21}$$

Calculating the characteristic photospheric pressure scale height, $h_{phot} \sim 2kT_{phot}R_1^2/GM_1 m_p$, and finding the depth in reference to an X-ray photosphere where $\tau_c \sim 1$, we obtain

$$d(\dot{m}(r)) = h_{phot} \ln(n_{phot} h_{phot} \sigma_c) = h_{phot} \ln \tau_{phot} \tag{22}$$

or

$$d(\dot{m}(r)) \sim R_1 (T_{phot}/T_s) \ln(\tau_e R_1/h). \tag{23}$$

For obscuration to be significant, $h_x \lesssim h_{phot} \ln \tau_{phot}$ and $4r_s \lesssim d(\dot{m}(r))$. These conditions are relatively straightforward to satisfy if $L/f(core) \geq 0.1 L_{Edd}$ with a characteristic core width of $r_s/R_1 \sim 10^{-4} - 10^{-3}$. However, for the azimuthally symmetric accretion profiles such as that shown in Figure 1b, the corresponding maximum core luminosity is $L_{core} \sim 0.1 L_{Edd}(10^{-3})^2/4 \sim 10^{30} - 10^{31}$ ergs/s. For the "trench" geometry, on the other hand, the maximum core luminosity is approximately $L_{core} \sim 0.1 L_{Edd}(10^{-3})/4 \sim 10^{33} - 10^{34}$ ergs/s. Clearly, the photospheric obscuration of arc-like structures, such as shown in Fig 1c, might explain a wide variety of phenomena associated with the hard X-ray flux: asymmetric and variable eclipse profiles, the "missing" hard X-rays in AM Her, and a consistent excess of soft X-ray flux observed in many AM Her sources (Beuermann, 1988*a*). Indeed, although the concept of photospheric obscuration post-dates the X-ray data, the sharp and irregular X-ray eclipses are strong evidence that the X-ray shock heights are comparable to those predicted for the bremsstrahlung-dominated Regime I.

4.2 Self-eclipse of the Optical Shock

Eclipses of the accretion shock by the phase-locked companion star are only confirmed in one source, E1114-182. Elsewhere in this volume, Schmidt describes two-color eclipse data which supports the notion of a large optical emission region, possibly a linear structure like Fig. 1c. However, the rotation of the white dwarf provides another eclipsing mechanism if the accretion region is small compared to the radius of the star, $h \ll R_1$. As the optical region passes over the limb, the optical light will slowly diminish and the observed circular polarization may change sign. While the finite width of the accretion region complicates interpretation of both photometric and polarimetric eclipse data, it is often possible to set upper limits on the height of the accretion shock.

The relationship between the polarimetric and photometric horizons for a shock height, $h \sim 0.1 R_1$, is shown in Fig. 6a. In this panel, the magnetic field is normal to the stellar surface, as it would be near the magnetic poles. The eclipse horizon is depressed below the polarimetric horizon or the tangent plane to the stellar suface by an angle, δ, given by

$$\delta = cos^{-1}\left(\frac{1}{1 + h/R_1}\right). \tag{24}$$

If $h \ll R_1$, a good approximation is

$$\delta \sim (2h/R_1)^{1/2}. \tag{25}$$

Thus, a small shock height, $h/R_1 \sim 0.01$, can result in a substantial depression of the eclipse horizon, $\delta \sim 0.14$ rad $\sim 8°$. As the cyclotron-emitting shock transits the limb of the star, the optical light will rapidly decline and the observed circular polarization will be observed to "reverse" for a portion of the 1-3 hr period,

$$\frac{\Delta P}{P} \sim \frac{(2h/R_1)^{1/2}}{2\pi}. \tag{26}$$

Liebert et al (1978) interpreted a particularly abrupt self- eclipse of VV Pup (Warner and Nather 1972) using this argument to obtain an upper limit to the optical shock of $h/R_1 < 0.01$. On the other hand, the somewhat longer polarization reversals observed in that source ($\Delta P/P \sim 0.07$, Liebert and Stockman 1979) yield a larger shock height, $h/R_1 \sim 0.1$. While both shock heights are compatible with the model results described in Section 2 and displayed in Fig. 2, the interpretation of the polarimetric eclipse may be seriously flawed. As anticipated by Stockman (1977) and modeled by Cropper and Warner (1986) and Wickramasinghe and Ferrario (1988, this volume), the magnetic field may not be normal to the stellar surface at the accretion shock. This situation is shown in Fig. 6b. Even for a shock of negligible height, the polarimetric horizon may be elevated substantially above the plane tangent to the stellar surface, yielding an observed polarimetric "reversal" at ingress, egress or both.

It is interesting to consider how large an effect we might expect. If the accretion stream is fully threaded at a distance comparable to the ballistic radius of closest approach, R_b, the accreted material will form a shock within an angle, θ of the magn pole given by the dipole approximation,

$$\theta \leq (2R_1/R_b)^{1/2}, \tag{27}$$

And the imbedded magnetic field will deviate less than δ_b from the stellar normal,

$$\delta_b \leq (R_1/2R_b)^{1/2}. \tag{28}$$

From the models of Lubow and Shu (1975), the radius of closest approach is $R_b/R_1 \sim 10$. Thus, the resulting polarization "reversal" may be significant, $\Delta P/P \sim 0.04$,and lead to an erroneous estimate of the shock height for $h/R_1 \lesssim 0.03$. We note, however, that multicolor polarization observations of VV Pup (Piirola *et al.* 1988), show no reversal in the U band compared to a large reversal in V. These data support the "height" interpretation rather than off-normal magnetic fields.

Despite the difficulties, we may be able to set reasonable upper limits to the optical shock height by noting the *lack* of an oberved polarization "reversal" in certain geometries. In Fig. 7, we indicate the expected duration of the "bright", uneclipsed phase for a point-like accretion shock for the complete range of magnetic colatitude and binary inclination (eg Brainerd and Lamb 1985, also Bailey and Axon 1980). In dotted lines, the duration of the bright phase is given for a shock height of $h/R_1 = 0.1$. The difference between the two geometries predicts the duration of the observed polarization "reversal" for the taller shock. Two qualitative effects of a significant shock height are evident: polarization "reversals" should be common, particularly when the active hemisphere is "up"; the fraction of unobservable systems (no bright period) becomes insignificant. Unfortunately our statistical sample is too small to address the second effect and most of the sources are either at too high or too low a colatitude to produce the polarization signature which would confirm a moderate shock height. AM Her, for instance, displays a prolonged polarization reversal in its active state which could be interpreted as either two active poles (Piirola *et al.* 1985) or a shock height, $h/R_1 \sim 0.05$. During its faint state, however, AM Her shows no polarization reversal (Latham *et al* 1979), implying a very low upper limit to the shock height, $h/R_1 < 0.01$, similar to the VV Pup photometric upper limit. DP Leo (E1114+182), with a magnetic colatitude of 103° and an inclination of 76° may be the best candidate for future study (Biermann *et al* 1985).

There is no unequivocable evidence for substantial heights ($h/R_1 \gtrsim 0.1$) of the optical shock. Some shocks might be expected to reach such a thickness (Section 2), particularly for lower field strengths. However, radiation transfer effects can generally be expected to reduce the shock thickness (Stockman and Lubenow 1987). Thus, the lower limits found in the bright state of VV Pup and the faint state of AM Her are consistent with the physical results and thin-shock approximation which are presented in Section 2 and which form the basis for the non-homogeneous shock models described in Section 3.

4.3 Seismology

Since the discovery of the AM Her systems in 1976, their strong photometric flickering has been often observed but seldom analyzed in depth. It is generally thought that the 10-100 s flicker noise discovered by Berg and Duthie (1975) and studied both in photometric, spectroscopic, and polarimetric detail by Bailey *et al* (1977), Margon and Szkody (1978), and Stockman and Sargent (1978) originates in the accretion shock but is due to instabilities in the upstream accretion flow– either near the secondary star or in the accretion threading region. However, without a quantitative theory describing either region, our progress in understanding these relatively slow variations has been slow.

Middleditch (1982) discovered a qualitatively different behavior in E1405-451 and AN UMa. In the former object, 5-10% variations can be observed with periods of approximately $P \sim 1-3s$. More remarkably, these oscillations can be quite distinct, often displaying one or two Fourier components with a coherence time of minutes or $Q > 30$ (Larsson 1984). Larsson has also discovered similar variations in VV Pup (Larsson 1987a) and EF Eri (Larsson 1987b). For all four objects, the range of fluctuations is similar and can be bounded by 0.3 Hz$< f <$1.3 Hz. Larsson (1984) found that the pulsed light in E1405-451 was typically red in color, although on one occasion, the color was neutral or blue in color (Larsson 1987a). Thus, the general assumption that the fluctuating light is due to cyclotron radiation has not been convincingly confirmed.

Instability studies of bremsstrahlung-dominated shocks have suggested that the observed pulsation range is feasible for low-mass white dwarfs ($M_1 < 0.4M_\odot$) and shock heights of $0.03 < h/R_1 < 0.2$ (Larsson 1987c). This connection, if correct, would be very important since it would permit an independent, detailed study of the AM Her accretion shocks in optical light. However, this interpretation of the observed fluctuations is not without difficulty:

a) The coherence of one or two Fourier modes and the strength of the fluctuations in E1405-451 requires that a major portion of the shock participates in the instability in a coherent fashion. However, in the context of a two-dimensional problem, the necessary coupling or synchronizing mechanisms may be either absent or critical to the correct interpretation. For instance, the instability may be occurring in a central, high density flow which, by fluctuating Compton cooling, affects the surrounding lower density regions.

b) Since the fluctuations are generally seen in red optical light, it is likely that the portion of the shock responsible for the red emission is cyclotron-dominated. As shown in Section 2.2, both important cooling rates, cyclotron radiation and electron-ion coupling, are very temperature dependent. For this reason, cyclotron-dominated shocks are not thought to be unstable to the same mechanism, although they may have instabilities due to other processes.

c) As noted by Larsson (1976), other potential origins for the fluctuations exist and must be examined. He suggests, for instance, that magnetohydrodynamic processes in the threading region may have the appropriate frequencies. The difficulty for all these theories is explaining the high quality factor, or long coherence time, particularly in the presence of strong, low frequency flickering. The best candidates will be those that evoke both a global synchronizing mechanism and an intrinsically sensitive physical characteristic, such as an photoionization edge. The current theories fail this criteria.

Clearly, further observations in both the optical and x-ray bands are required to establish the origins of the fast optical fluctuations and their promise for studying the structure of the magnetic variable accretion shocks.

REFERENCES

Bailey, J., Mason, K., and Parkes, G. E. 1977, *M.N.R.A.S.*, **166**, 113.

Bailey, J. and Axon, D. J. 1980, *M.N.R.A.S.*, **194**, 187

Bailey, J., 1988, this volume.

Berg, R. A. and Duthie, J. G. 1977, *Ap. J.*, **211**, 859.

Beuermann, K., Stella, L., and Patterson, J. 1987 *Ap. J.*, **316**, 360.

Beuermann, K. 1988*a*, this volume.

Beuermann, K. 1988*b*, in *The Physics of Compact Objects: Theory Versus Observations*, Reidel, in press.

Biermann, P., Schmidt, G. D., Liebert, J., Stockman, H. S., Tapia, S., Kuhr, H., Strittmatter, P. A. S., West, S., and Lamb, D. Q. 1985, *Ap. J.*, **293**, 303.

Brainerd, J. J., and Lamb, D. Q. 1985, in *Cataclysmic Variables and Low-Mass X-ray Binaries*, ed. J. Patterson and D. Q. Lamb (Cambridge: Reidel), p. 247.

Cropper, M., and Warner, B. 1986, *M.N.R.A.S.*, **220**, 633.

Dulk, G. A., and Marsh, K. A. 1982, *Ap. J.*, **259**, 350.

Imamura, J. N., Durisen, R. H., Lamb, D. Q., and Weast, G. J. 1987, *Ap. J.*, **313**, 298.

Kaluzny, J. and Semeniuk, I. 1987, *Acta Astron.*, **37**, in press.

Kaluzny, J. and Chlebowski 1988, *Ap. J. (Letters)*, in press.

Kemp, J., Swedlund, J. and Wolstencroft, R. 1974, *Ap. J. (Letters)*, **193**, L15.

Lamb, D. Q., and Masters, A. R. 1979, *Ap. J. (Letters)*, **234**, L117.

Lamb, D. Q. 1985, in *Cataclysmic Variables and Low-Mass X- ray Binaries*, ed. J. Patterson and D. Q. Lamb (Cambridge: Reidel), p. 179.

Lamb, D. Q., 1988, this volume

Lanning, H. H. and Semeniuk, I. 1981, *Acta Astron.*, **31**, 175.

Larsson, S., 1985, *Astron. Astrophys*, **145**, L1.

Larsson, S., 1987a, *Astrophys. and Space Sci*, **130**, ed. Remeis-Sternworte, Reidel. 187.

Larsson, S., 1987b, *Astron. Astrophys*,**181**, L15.

Larsson, S., 1987c, "Proceedings of the COSPAR/IAU Symposium on the Physics of Compact Objects: Theory versus Observations."

Latham, D. W., Liebert, J., and Steiner, J. E. 1981, *Ap. J.*, **246**, 919.

Liebert, J., Stockman, H. S., Angel, J. R. P., Woolf, N. J., Hege, E. K., and Margon, B. 1978, *Ap. J.*, **219**, 201.

Liebert, J. and Stockman, H. S. 1979, *Ap. J.*, **229**, 652.

Liebert, J. and Stockman, H. S. 1985, in *Cataclysmic Variables and Low-Mass X-ray Binaries*, ed. J. Patterson and D. Q. Lamb (Cambridge: Reidel), p. 151.
Lubow, S. H., and Shu, F. H. 1975, *Ap. J.*, **198**, 383.
Margon, B. and Szkody, P. 1978, private communication.
Mason, K. O., Middleditch, J., Cordova, F. A., Jensen, K. A., Reichert, G., Murdin, P. G., Clark, D. and Bowyer, S., 1983, *Ap. J.*, **264**, 575.
Masters, A. R. 1978, Ph.D. Dissertation, Univ. Ill.
Middleditch J., 1982, *Ap. J. (Letters)*,**257**, L71.
Piirola, V., Vilhu, O., Kyrolainen, J., Shakhovskoy, N. M., and Efimov, Y. S. 1985, ESA SP-236, 256.
Piirola, V. 1988, this volume.
Piirola, V., Reiz, A. and Coyne, G. V. 1988, *Astron. Astrophys.* submitted.
Schmidt, G. D., Stockman, H. S., and Margon, B. 1981, *Ap. J.(Letters)*, **243**, L157.
Schmidt, G. D., Stockman, H. S., and Grandi, S. A. 1983, *Ap. J.*, **271**, 735.
Schmidt, G. D. 1988, this volume.
Stockman, H. S., 1977,*Ap. J.(Letters)*, **218**, L57.
Stockman, H. S. and Sargent, T. A. 1979, *Ap. J.*, **227**, 197.
Stockman, H. S., and Lubenow, A. F. 1987, *Astrophysics and Space Science*, **131**, 607.
Tapia, S. 1977, *Ap. J.(Letters)*, **212**, L125.
Visvanathan, N. and Wickramasinghe, D. T. 1979, *Nature*, **281**, 47.
Warner, B., and Nather, R. E. 1972, *M.N.R.A.S.*, **156**, 305.
Wickramasinghe, D. T., and Ferrario, L. 1988, *Ap. J.*, in press.
Wickramasinghe, D. T., 1988, this volume.

FIGURE CAPTIONS

Figure 1. Schematic illustrations of three different shock geometries. The upper panel (a)represents the typical "pillbox" geometry of the homogeneous shock and the basic shock terminology. The middle panel (b) represents the radially symmetric, non-homogeneous shock. High density flow in the core transitions smoothly to a low-density accretion flow in the wings which produce much of the observed optical cyclotron flux. The bottom panel (c) illustrates a more linear structure in which the the accretion shock forms a sheath or arc-like structure.

Figure 2. The relative shock height for a range of accretion luminosities. The four heavy lines indicate the relative shock height for 0.4 and $1.0 M_{\odot}$ white dwarfs and two field values, B =10,30 MG. Contours labeled $10^{32}, 10^{33}$, and 10^{34} indicate the upper limits to the thin shock approximation for radially symmetric shocks with the corresponding luminosity (ergs/s).

Figure 3. The complete energy distribution for a gaussian and quadratic accretion profile. The model parameters are $M_1 = 0.8 M_{\odot}$, $L = 10^{33}$ erg/s, $B = 20$ MG, $< L/f >= 10^{38}$ erg/s for both models. From Stockman and Lubenow (1987).

Figure 4. The shock characteristics versus radius, r, for the quadratic accretion profile described in Figure 3. From Stockman and Lubenow (1987).

Figure 5. A cross section of a high density accretion core. The depression of the photosphere is due to accretion ram pressure.

Figure 6. Two scenarios which produce polarization "reversals." The left panel (a) indicates the depression of the eclipse horizon due to significant shock height. The right panel (b) shows the effect of non-normal magnetic field lines. Note the beaming of the polarization horizon into the stellar surface on one side of the shock.

Figure 7. The effect of column height on shock visibility. The solid lines indicate the fraction of the period in which a one-pole accretion shock would be visible. The dotted lines indicate the "bright" phase fraction for a shock height of $h/R_1 = 0.1$. Note that, in this case, accretion on the "South Pole" can be visible for a large fraction of the period.

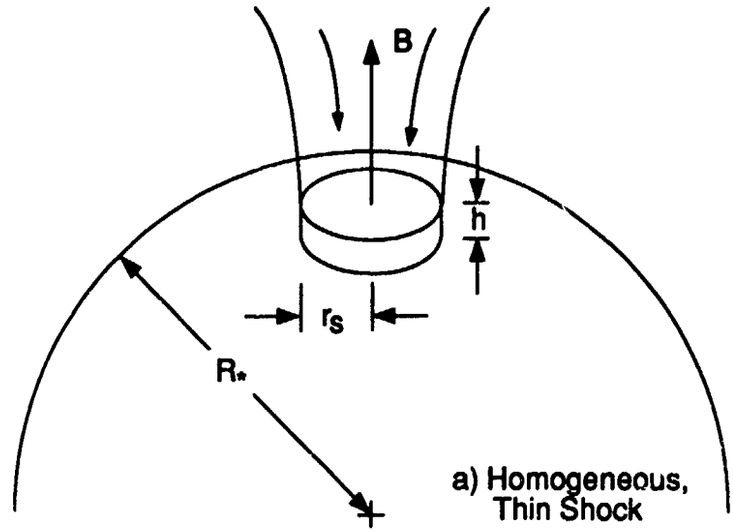
B
h
r_s
R_*
a) Homogeneous,
Thin Shock

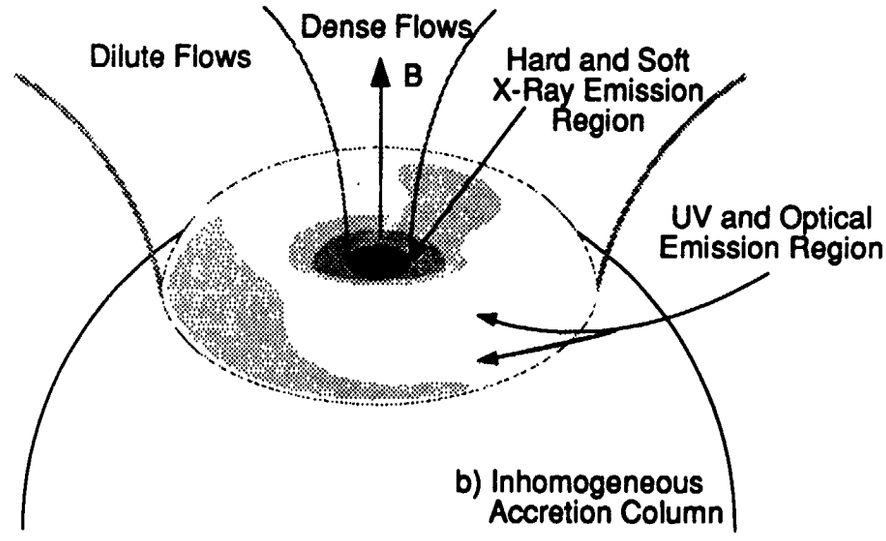
Dense Flows
Dilute Flows
B
Hard and Soft
X-Ray Emission
Region
UV and Optical
Emission Region
b) Inhomogeneous
Accretion Column

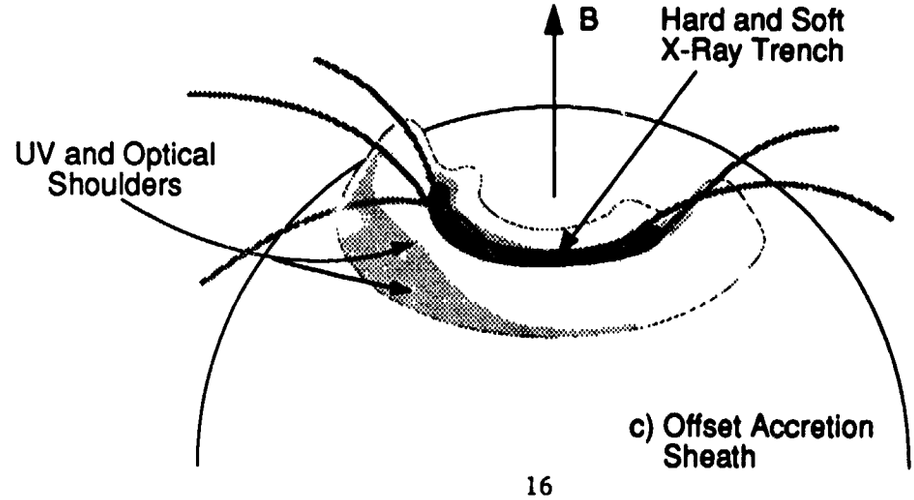
B
Hard and Soft
X-Ray Trench
UV and Optical
Shoulders
c) Offset Accretion
Sheath

Figure 1.

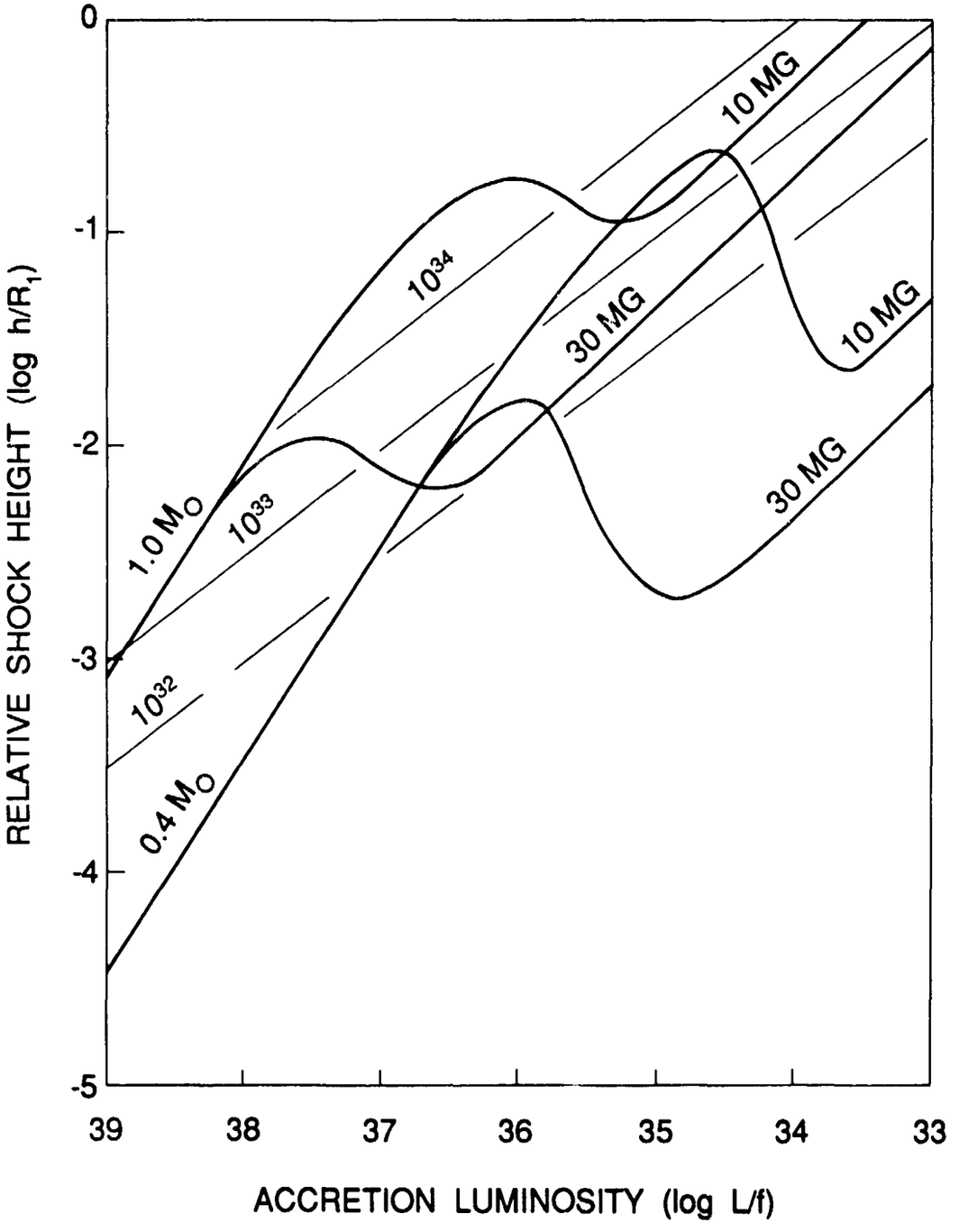
RELATIVE SHOCK HEIGHT (log h/R1)
ACCRETION LUMINOSITY (log L/f)
0
-1
-2
-3
-4
-5
39
38
37
36
35
34
33
10 MG
30 MG
10 MG
30 MG
10^34
10^33
10^32
1.0 MO
0.4 MO

Figure 2.

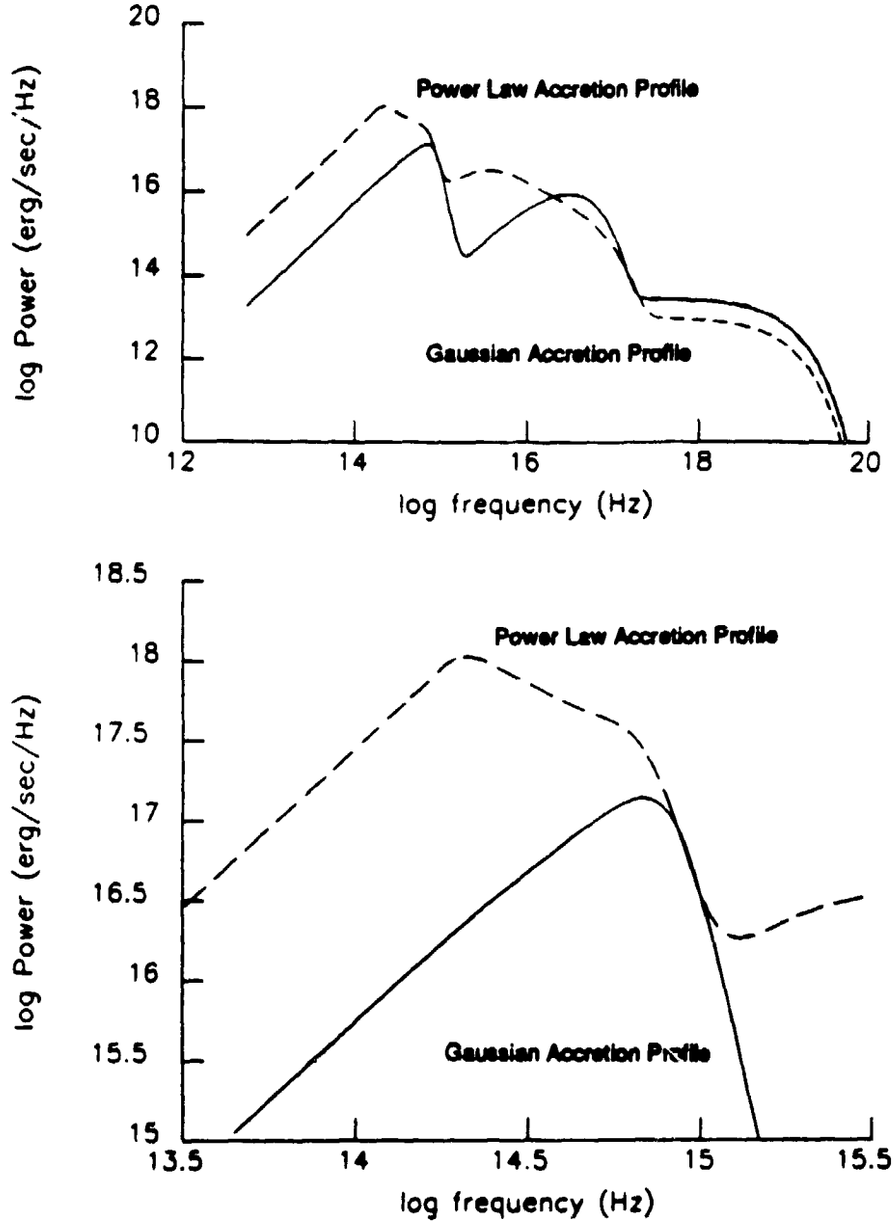
log Power (erg/sec/Hz)
20
18
16
14
12
10
12
14
16
18
20
log frequency (Hz)
Power Law Accretion Profile
Gaussian Accretion Profile
log Power (erg/sec/Hz)
18.5
18
17.5
17
16.5
16
15.5
15
13.5
14
14.5
15
15.5
log frequency (Hz)
Power Law Accretion Profile
Gaussian Accretion Profile

Figure 3.

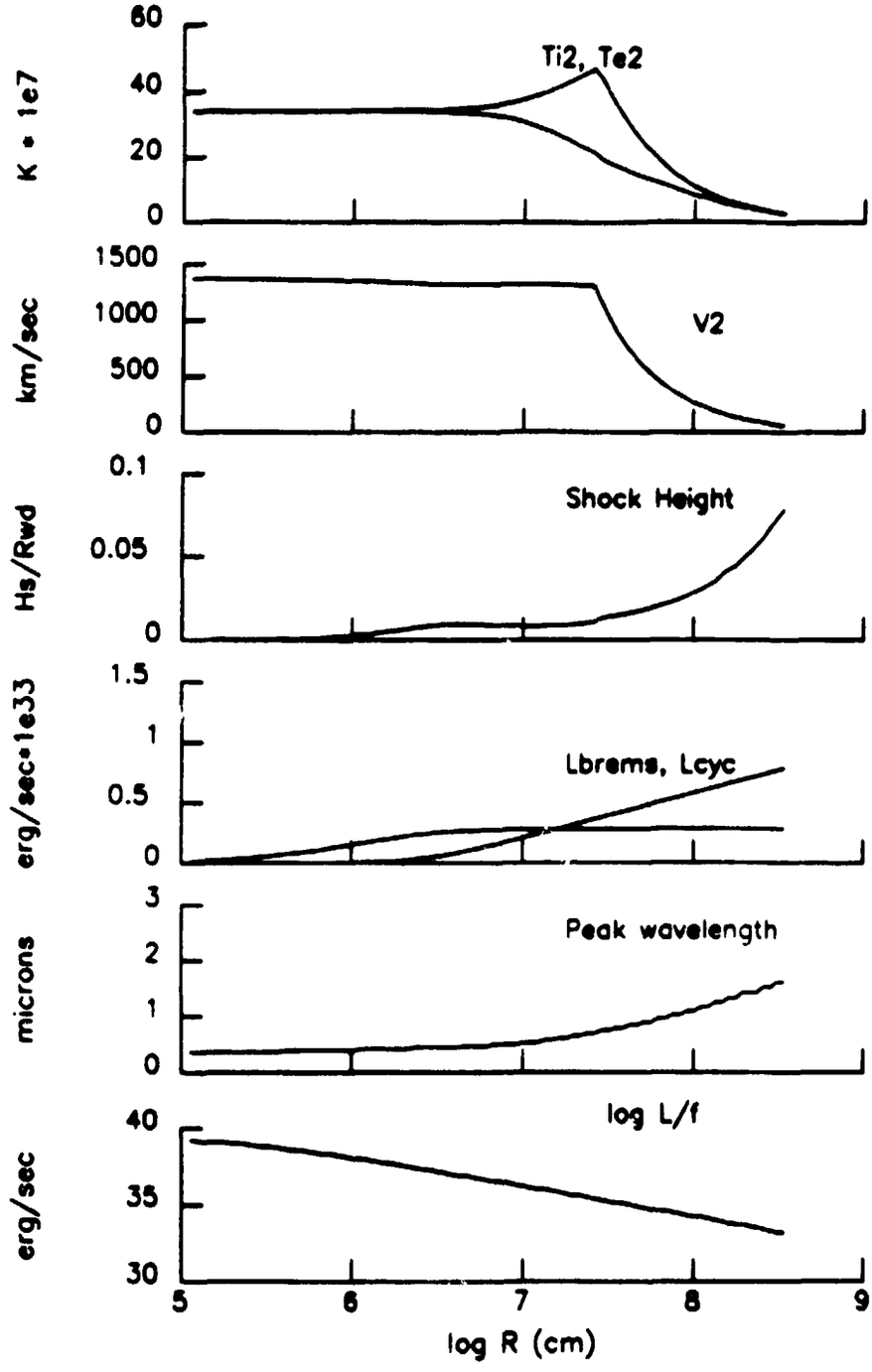
K * 1e7
60
40
20
0
Ti2, Te2
km/sec
1500
1000
500
0
V2
Hs/Rwd
0.1
0.05
0
Shock Height
erg/sec*1e33
1.5
1
0.5
0
Lbrems, Lcyc
microns
3
2
1
0
Peak wavelength
erg/sec
40
35
30
log L/f
5
6
7
8
9
log R (cm)

Figure 4.

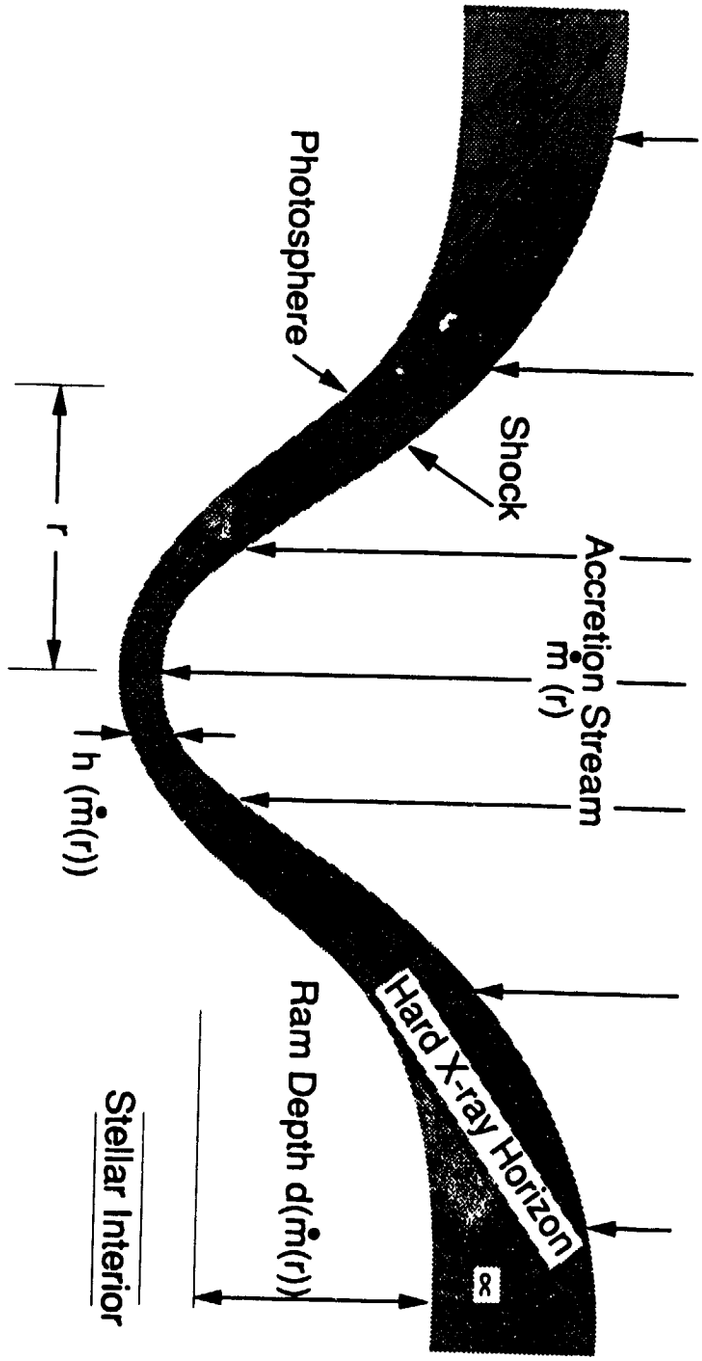
Photosphere
Shock
Accretion Stream
$\dot{m}$ (r)
r
h ($\dot{m}$(r))
Hard X-ray Horizon
Ram Depth d($\dot{m}$(r))
Stellar Interior

Figure 5.

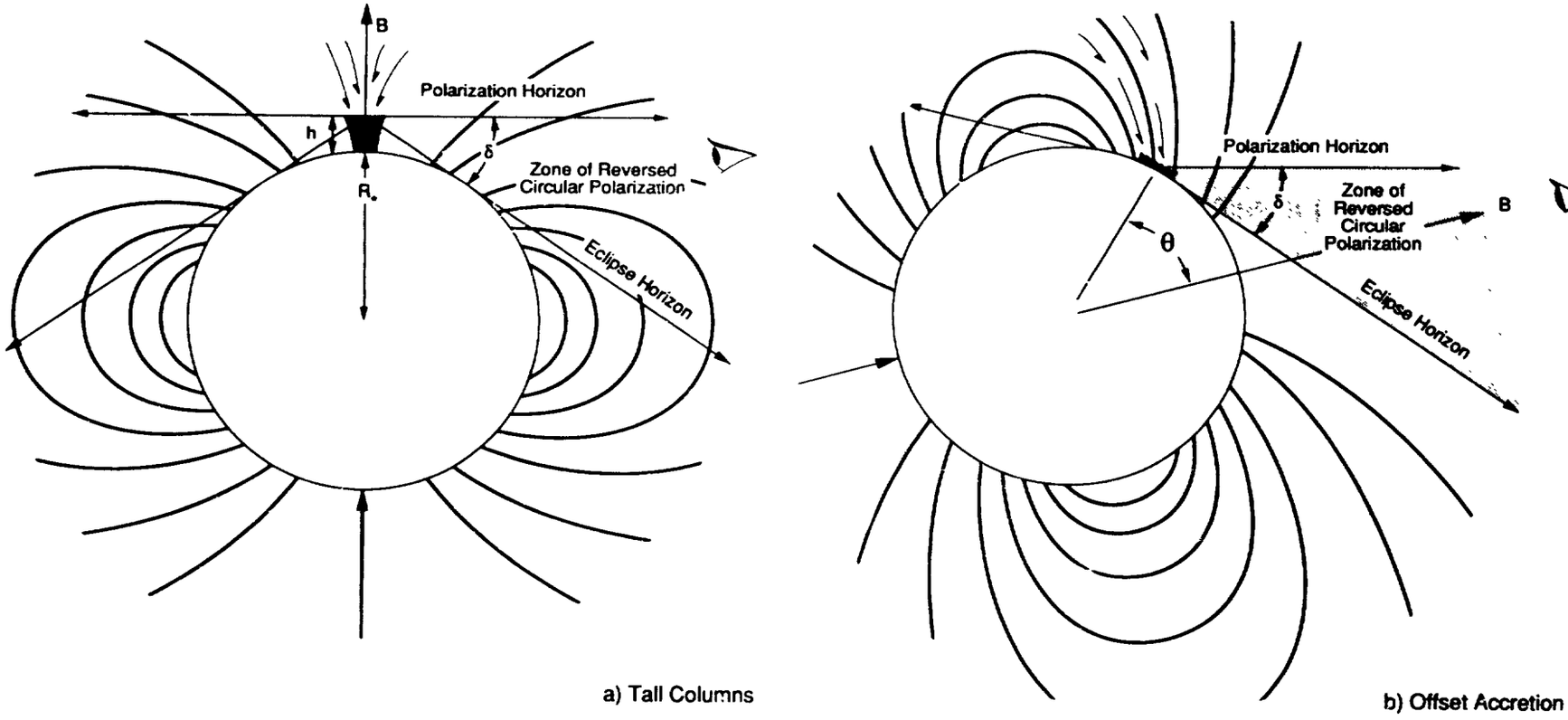
B
Polarization Horizon
h
δ
Zone of Reversed
Circular Polarization
R*
Eclipse Horizon
a) Tall Columns
Polarization Horizon
δ
Zone of
Reversed
Circular
Polarization
B
θ
Eclipse Horizon
b) Offset Accretion

Figure 6.

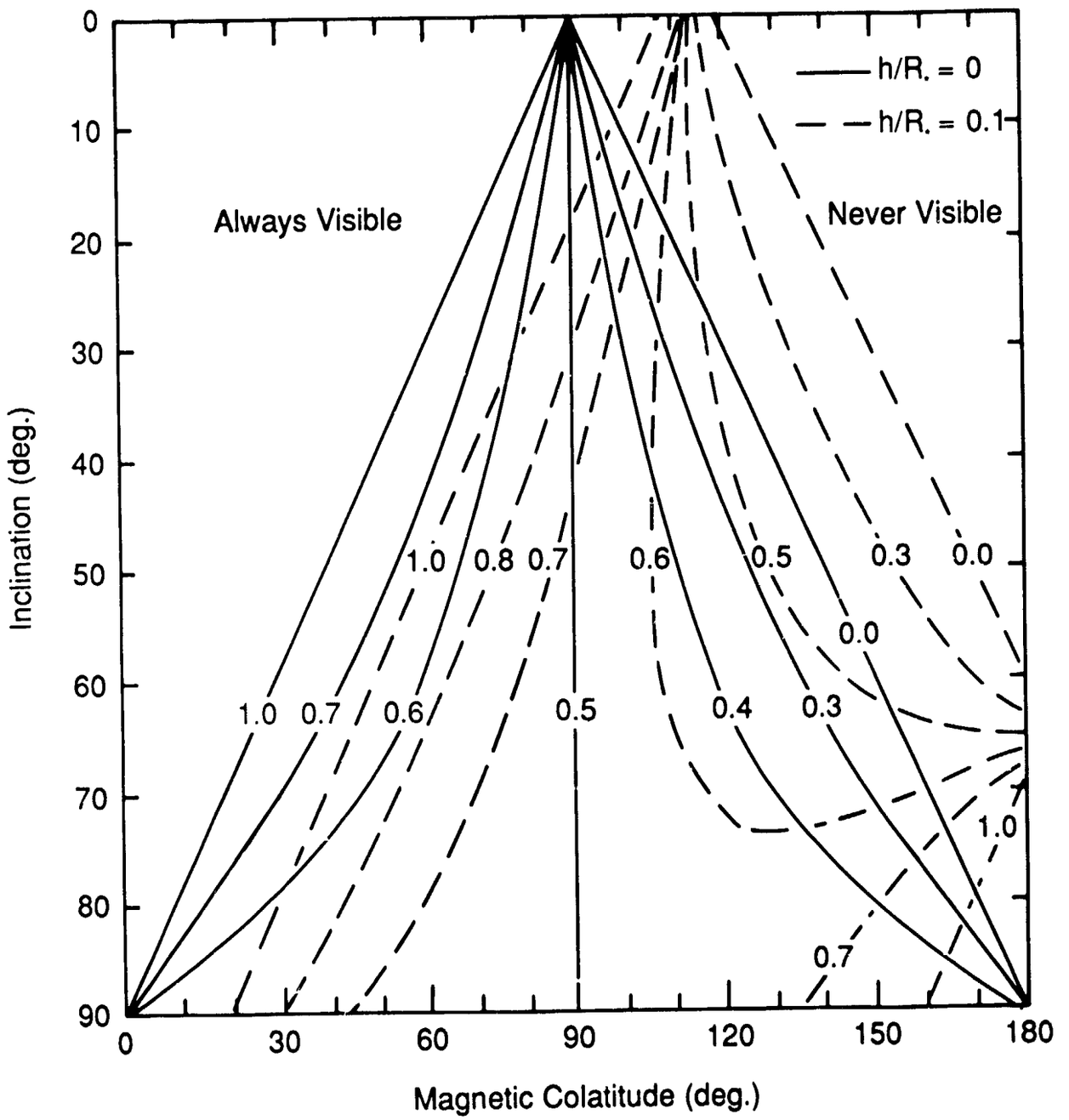
h/R. = 0
h/R. = 0.1
Always Visible
Never Visible
Inclination (deg.)
Magnetic Colatitude (deg.)
0
10
20
30
40
50
60
70
80
90
0
30
60
90
120
150
180
1.0
0.8
0.7
0.6
0.5
0.3
0.0
1.0
0.7
0.6
0.5
0.4
0.3
0.0
1.0
0.7

Figure 7.